Proc. Natl. Acad. Sci. USA
Vol. 91, pp. 9784–9788, October 1994
Physiology

Imaging nuclear pores of aldosterone-sensitive kidney cells by atomic force microscopy

HANS OBERLEITHNER*†, EDNA BRINCKMANN*, ALBRECHT SCHWAB*, AND GEORG KROHNE‡

*Department of Physiology, University of Würzburg, Röntgenring 9, 97070 Würzburg, Germany; and ‡Division of Electron Microscopy, Theodor Boveri Institute, University of Würzburg, Am Hubland, 97074 Würzburg, Germany

Communicated by Robert W. Berliner, June 14, 1994

ABSTRACT **In nuclei of renal target cells, aldosterone enhances transcriptional activity followed by the translocation of specific RNA molecules across the nuclear envelope. Trafficking between cell nucleus and cytoplasm occurs via nuclear pore complexes (NPCs) located in the double-layered nuclear envelope. We investigated the nucleocytoplasmic transport route by structure–function analysis at subcellular level in quiescent and aldosterone-stimulated cells. With atomic-force microscopy (AFM) we imaged individual pores of the nuclear surface of cultured kidney cells and related the number of pores per μm^2 to nuclear envelope conductance (G_n, per μm^2) evaluated electrically by current injection into the isolated nucleus. NPCs were equally distributed resembling "donut-like" structures with outer diameters of 134 ± 12 nm ($n = 50$), each equipped with a central channel. Six hours of aldosterone exposure (0.1 μM) increased the number of NPCs per μm^2 of nuclear surface from 7.4 ± 0.4 to 9.8 ± 0.4 ($n = 12$; $P < 0.01$). At the same time G_n rose from 6900 ± 520 to 9600 ± 610 $pS/\mu m^2$ paralleled by an increase of the intranuclear electrical potential from −2.8 ± 0.2 to −6.2 ± 0.4 mV ($n = 18$; $P < 0.01$). Assuming that NPCs represent the sole conductive pathway in the nuclear envelope, we calculate a mean single NPC conductance of 932 and 980 pS, in the absence and presence of aldosterone, respectively. We conclude that aldosterone facilitates nucleocytoplasmic transport by increasing the number of NPCs but not by modifying their biophysical properties. Possibly, aldosterone controls similar transport mechanisms in both plasma membrane and nuclear envelope.**

Steroid hormones such as aldosterone act by binding to intracellular receptors forming hormone–receptor complexes. Hormone interaction converts the receptor into a transcriptional enhancer. Specific RNA molecules are synthesized that must cross the boundary separating the nucleus from the cytoplasm (1). There is general agreement that nuclear pore complexes (NPCs) serve as the supramolecular basis for nucleocytoplasmic transport (2, 3). High-resolution scanning electron microscopy combined with digital-imaging techniques disclosed the basic architectural framework of an individual NPC (4, 5). To gain access to the structure, dynamics, and function of NPCs, we applied atomic-force microscopy (AFM) and electrophysiology to nuclei of aldosterone-sensitive Madin–Darby canine kidney (MDCK) cells. The AFM technique allows three-dimensional imaging of biostructures at the nanometer level (6–8). Here we imaged individual NPCs *in situ*, with emphasis on the visualization of the central channel. We quantified the number of NPCs per nucleus of cells grown under aldosterone-depleted and -stimulated conditions. In parallel, we electrically measured nuclear envelope potential and conductance with the goal to learn more about the physiology of NPCs.

The publication costs of this article were defrayed in part by page charge payment. This article must therefore be hereby marked "*advertisement*" in accordance with 18 U.S.C. §1734 solely to indicate this fact.

METHODS

Cell Culture and Nuclei Preparation. The aldosterone-sensitive cell clone C11 (9), derived from MDCK wild-type cells (American Type Culture Collection) was grown in minimal essential medium (MEM) with Earle's salts, nonessential amino acids, and L-glutaminic acid (Biochrom, Berlin). The medium was supplemented with 10% (vol/vol) fetal calf serum and 26 mM $NaHCO_3$. Cells were grown to confluency at 37°C in a humidified atmosphere of 5% CO_2 in air.

For the AFM experiments, we prepared the nuclear surface *in situ* as follows. Cells grown to confluent monolayers on thin glass coverslips (round; diameter, 15 mm) were washed in Hepes-buffered Ringer solution, then shortly exposed to a strongly hypotonic solution (10 mM Tris buffer, pH 7.2), and incubated for a few minutes in Ringer solution containing 1% Triton X-100. This stepwise procedure dissociates the plasma membrane from the cytoskeleton and dissolves the lipidic structures of the plasma membrane and the nuclear envelope. The monolayer was again washed in Ringer solution, fixed by glutaraldehyde (1% fixative in Hepes-buffered Ringer solution), and, after rinsing in distilled water, air-dried.

For the electrical experiments, we needed cell nuclei with an intact nuclear envelope. For this purpose we isolated nuclei with the sucrose/citric acid method as described in detail (10, 11). In short, cells were harvested from a confluent monolayer by trypsination, suspended in moderately hypotonic solution (70 mM NaCl/10 mM Tris buffer, pH 7.2), and centrifuged at room temperature for 5 min at 500 × *g*. Then, the cell pellet was suspended in strongly hypotonic solution (10 mM Tris buffer, pH 7.2) and homogenized with 40 strokes of a tight-fitting Teflon pestle (at 800 rpm) in a glass Potter homogenizer vessel immersed in ice. The protease inhibitor phenylmethylsulphonyl fluoride (0.1 mM) was present during homogenization to prevent proteolysis of histones. The homogenate was then centrifuged at 4°C for 5 min at 700 × *g*. The pellet was resuspended in 5 ml of ice-cold solution of sucrose (2.5 mol/liter) in 1.5% (wt/vol) citric acid and again homogenized with 5 strokes (at 800 rpm). The homogenate was then underlayered with 5 ml of ice-cold 0.88 M sucrose in 1.5% citric acid and centrifuged at 4°C for 10 min at 1000 × *g*. Thereafter, the isolated nuclei were suspended in a buffered salt solution with a composition mimicking the cytosolic salt concentrations. This cytosolic buffer was composed of 120 mM KCl, 10 mM NaCl, 2 mM $MgCl_2$, 1.1 mM EGTA, 0.1 mM $CaCl_2$, 10 mM Hepes (pH 7.4). In this solution the isolated nuclei were transferred on glass coverslips coated with poly(L-lysine). Nuclei were now ready for electrical measurements.

Nuclear Envelope Potential and Conductance Measurements. All electrical measurements on isolated nuclei were

Abbreviations: NPC, nuclear pore complex; AFM, atomic-force microscopy.

†To whom reprint requests should be addressed.

performed in cytosolic Ringer solution (see above) on the stage of an inverted microscope equipped with high-resolution interference contrast (IM 35, Zeiss). The technical details of intranuclear potential measurements in isolated nuclei have been described (11). For the evaluation of the total electrical conductance of the nuclear envelope, two microelectrodes (filled with 1 M KCl; 50-MΩ input resistance) were inserted into a nucleus. The negative intranuclear potential clearly indicated successful impalements. One microelectrode was used for current injections (1–5 nA; repetitive pulses of 200-ms duration applied every 2 s), while the other microelectrode picked up the corresponding voltage changes. The bath solution with a composition mimicking the cytosolic salt concentration was electrically grounded by a low-resistance Ag/AgCl agar bridge. According to Ohm's law, the total nuclear conductance could be calculated. Since isolated nuclei could be assumed to be approximately spherical (11), we measured the individual nuclear radii, calculated the surface, and related the specific nuclear envelope conductance to surface area ($G_n/\mu m^2$).

AFM. The application of AFM on soft biological samples has been described in various reports in detail (7, 8, 12). In short, we used a NanoScope III (L.O.T.-Oriel, Darmstadt, Germany) equipped with either a 125 × 125 μm or a 14 × 14 μm AFM stage. The nuclear preparation (either the fixed monolayer or the isolated nuclei) was mounted on top of the x,y,z translator and scanned with V-shaped cantilevers (spring constants of about 0.12 N/m, integral silicon nitride tips). By means of a conventional light microscope, we identified individual nuclei and directed the scanner manually close to the nuclear surface. Then, by motor-driven and electronically directed devices, the tip was lowered until it engaged the nuclear surface. Engagement of the tip started the scanning process. For the evaluation of the number of pores per μm^2, we randomly selected 10 different areas per nucleus of 1 μm^2, counted the number of NPCs on the computer screen, and calculated the mean number for each nucleus. Twenty-four nuclei were investigated (from 12 hormone-depleted and 12 hormone-supplemented cells); these mean values ± SEM are reported (Table 1).

Imaging the structure of a single NPC demanded fine-tuning of the scanning process. This comprised mainly the adjustment of the force between tip and sample below 10 nN, the reduction of the scan rate to values below 5 Hz, and the increase of the scan lines per area to 512. Thus, imaging a single pore took several minutes. Raw data could be stored and analyzed after the experiment. Software was supplied from the manufacturer (Digital) that allowed us to pitch, rotate, and modify the z scale of the image for complete analysis of the sample.

Table 1. AFM and electrophysiology of MDCK cell nuclei

Parameter	Control	Aldosterone
AFM (12 nuclei)		
Nuclear surface, μm^2	205 ± 17	212 ± 19
Pores per μm^2	7.4 ± 0.4	9.8 ± 0.4*
Pores per nucleus	1482 ± 85	2020 ± 94*
Electrophysiology (18 nuclei)		
Nuclear voltage, mV	−2.8 ± 0.2	−6.2 ± 0.4*
G_n, nS/μm^2	6.9 ± 0.5	9.6 ± 0.6*
G_{npc}, pS	932	980
Electr. pore diam., nm	10.6	10.9

Control signifies serum-free for 24 hr. Aldosterone signifies serum-free for 18 hr followed by 6 hr of exposure to 0.1 μM aldosterone. The negative nuclear voltage indicates an electrically negative nucleoplasm in reference to the grounded cytosolic solution. G_n is the total nuclear envelope conductance, and G_{npc} is the single nuclear pore conductance estimated from G_n and the number of pores per area. The electrical pore diameter (d) was estimated from the equation $d = 2[(\rho \cdot l \cdot G_{npc})/\pi]^{1/2}$. In this equation ρ is the resistivity of the cytosolic solution (100 Ω·cm) and "l" is the estimated length of the pore (80 nm). *, A statistically significant difference ($P < 0.01$) to the corresponding control value.

Evaluation of Nuclear Surface Area. For the evaluation of the number of pores per nucleus and of the electrical conductance per μm^2 of nuclear surface, it was necessary to measure the absolute surface areas of individual nuclei. We used two different approaches. In one approach, nuclei of the *in situ* preparation resembled approximately segments of spheres. The surface area of the basis ($a^2\pi$; a = radius of the segment's circular base) and the height (h) of the sphere's segment could be exactly measured by AFM. According to the equation: $S = \pi(a^2 + h^2) + a^2\pi$, the nuclear surface ($S$) could be calculated. To be able to apply the equation, we chose nuclei with approximately circular outlines. The mean data of these measurements are displayed in Table 1. The other approach was based on isolated nuclei used for the electrical measurements. This method has been described (11). A suspension of nuclei was pipetted rapidly onto an appropriate poly(L-lysine)-coated glass coverslip forming the bottom of a small superfusion chamber. Nuclei immediately stuck to the glass surface and could be superfused on the stage of an inverted microscope (IM 35; Zeiss). With Nomarsky optics the outer borders of the nuclei were clearly visible. The nuclear surface was analyzed by means of a video-imaging system (Java; Jandel, Corte Madera, CA) that allowed processing of the videotaped images. There, the images of the nuclei were digitized and contrast-enhanced. The outlines of an individual nucleus in focus could be traced by a manually driven digital cursor. From the nuclear circumference, the area (i.e., the cross-sectional area of a sphere) was calculated. Assuming that this area presented a circle, we calculated the radius (a) and used it to evaluate the nuclear surface (S) according to the equation: $S = 4a^2\pi$. Optical sectioning as described (11) was performed to verify that nuclei were indeed spherical. In isolated nuclei of either hormone-depleted or aldosterone-supplemented cells, we measured surface areas of 192 ± 15 (n = 64) and 187 ± 14 μm^2 (n = 69), respectively. These mean values were not significantly different from the values obtained in the *in situ* preparation by AFM (Table 1). Nevertheless, all electrical conductance measurements were related to the individual surface of the isolated nucleus under study.

RESULTS

The response of renal target cells to aldosterone is pleiotropic, involving proliferation, differentiation, and directed transport of ions across the epithelium (13, 14). Sustained action is based on nuclear transcription of hormone-specific genes, translocation of the transcripts through the NPCs from nucleus to cytoplasm, and, finally, *de novo* synthesis of aldosterone-induced proteins serving directly as plasma membrane transporters or more indirectly as intracellular mediators of transepithelial transport. We applied the AFM technique to visualize individual NPCs on the cytoplasmic surface of hormone-depleted and hormone-supplemented MDCK cell nuclei. Fig. 1 shows images of the apical surface of one individual nucleus. Hypotonic shock and rigorous detergent treatment completely removed the plasma membrane, leaving behind a denudated nucleus attached to the coverslip (Fig. 1*a*). The nucleolus is clearly visible as a light spot protruding from the center of the nucleus. Remnants of the cytoskeleton are visible in the close vicinity of the nuclear outlines. Reducing the scan area to about 8 μm^2 discloses individual NPCs on the nuclear surface (Fig. 1*b*). For orientation, a minor portion of the nucleolus can be seen at the right upper corner of the image. Further reduction of the scan area generates an image in which the NPCs can be easily detected and distinguished from holes in the preparation that

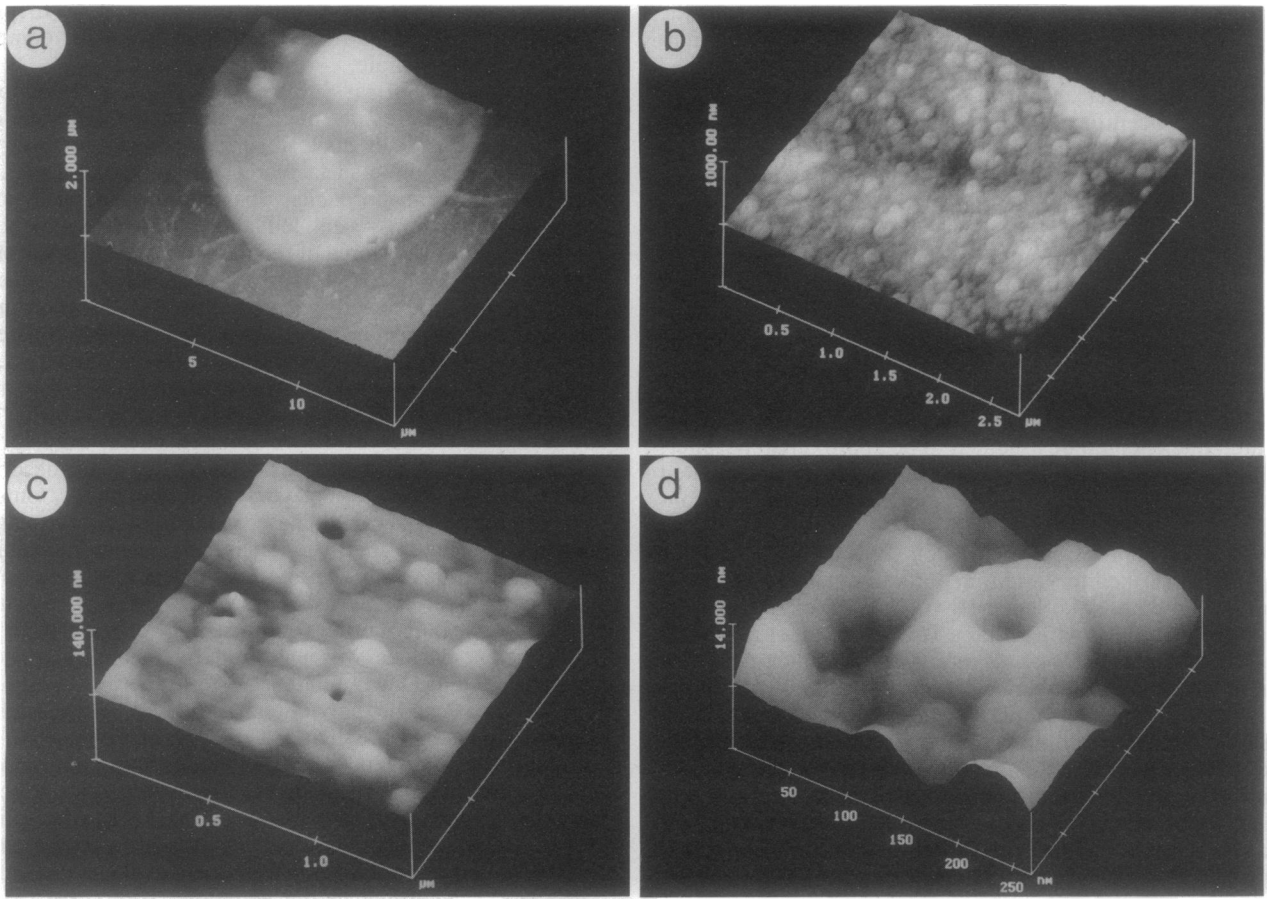

FIG. 1. Images of the nuclear surface of a MDCK cell. (*a*) Apical nuclear surface after detergent treatment. The light spot in the center represents the nucleolus. (*b*) Patch (8 μm^2) of nuclear surface. NPCs can be clearly seen. A fraction of the nucleolus is visible in the right upper corner. (*c*) Patch (2.5 μm^2) of nuclear surface. The light and prominent spots represent NPCs, whereas the dark holes represent possible artefacts caused by the rigorous detergent treatment. (*d*) Individual NPC with clearly visible central channel.

represent artefacts most likely induced by detergent treatment (Fig. 1*c*). A single NPC with its centrally located channel is displayed in Fig. 1*d*. About 2500 patches of the size of this scan area establish the nuclear envelope. NPC images obtained by the AFM technology can be quite different. Two possible variants are depicted in Fig. 2. The ring-like feature facing the cytosol was usually found more or less segmented. Sometimes up to eight subunits could be detected as proposed in the literature (4, 5). The size and structure of an individual NPC can vary considerably. Outer diameters of the cytosolic rings were between 100 and 300 nm. We analyzed 50 NPCs and calculated a mean value of 134 ± 12 nm. Examples for large and small NPCs are shown in Fig. 2 *a*/*b* and *c*/*d*, respectively. Because of this scatter, we were unable to detect any differences in the NPC structure of aldosterone-depleted versus -supplemented cells. Also, it remains unclear whether the scatter reflects biological variations or rather technical problems.

Previous work has established that a "central structure" is present within the NPC. It has been named the "transporter," as it appears to define the macromolecular transport channel for a variety of organic substrates (15, 16). By elegant studies applying three-dimensional cryoelectron microscopy, an elongated centrally tapered cylinder was visualized, lending support to the so-called macromolecular lock hypothesis. In this model, it is suggested that substrate passage across the nuclear envelope may require gating mechanisms within the central channel (15, 16). With the AFM we could detect structures inside the central channel (Fig. 2 *b* and *d*). They were already detectable a few nanometers below the outer rim of the cytoplasmic coaxial ring. These structures could represent the cytosolic face of the transporter, which is supposed to control transenvelope traffic of macromolecules.

Electrical transenvelope potential and conductance measurements were performed in isolated nuclei of MDCK cells bathed in a solution mimicking the cytosol. This experimental model has been used (11) to evaluate the transenvelope potential in response to inorganic ions in MDCK cells. The cell nuclei investigated were isolated from MDCK cells cultured in the absence (control) or presence of 0.1 μM aldosterone. The electrical data are presented in Table 1. Intranuclear voltage was found electrically negative in reference to the cytosol, confirming previous results (11). Hormone treatment for 6 hr significantly increased intranuclear electrical potential. At the same time, nuclear envelope conductance increased by about one-third. Taking into account the number of pores per nucleus (see Table 1), we could estimate the single-pore conductance for both hormone-deprived and hormone-supplemented cells. Apparently, the aldosterone-induced increase of nuclear pore frequency matched the rise in G_n, indicating that single G_{npc} was not affected by the hormone. If one assumes that the central channel of an individual NPC had a cylindrical shape (15), the electrical diameter of this channel could be calculated (for details see the legend of Table 1). It was about 11 nm for both hormone-depleted and hormone-supplemented conditions.

DISCUSSION

There is general agreement that the nuclear envelope has a barrier function selectively separating the genome from other cytosolic compartments. Experimental evidence clearly in-

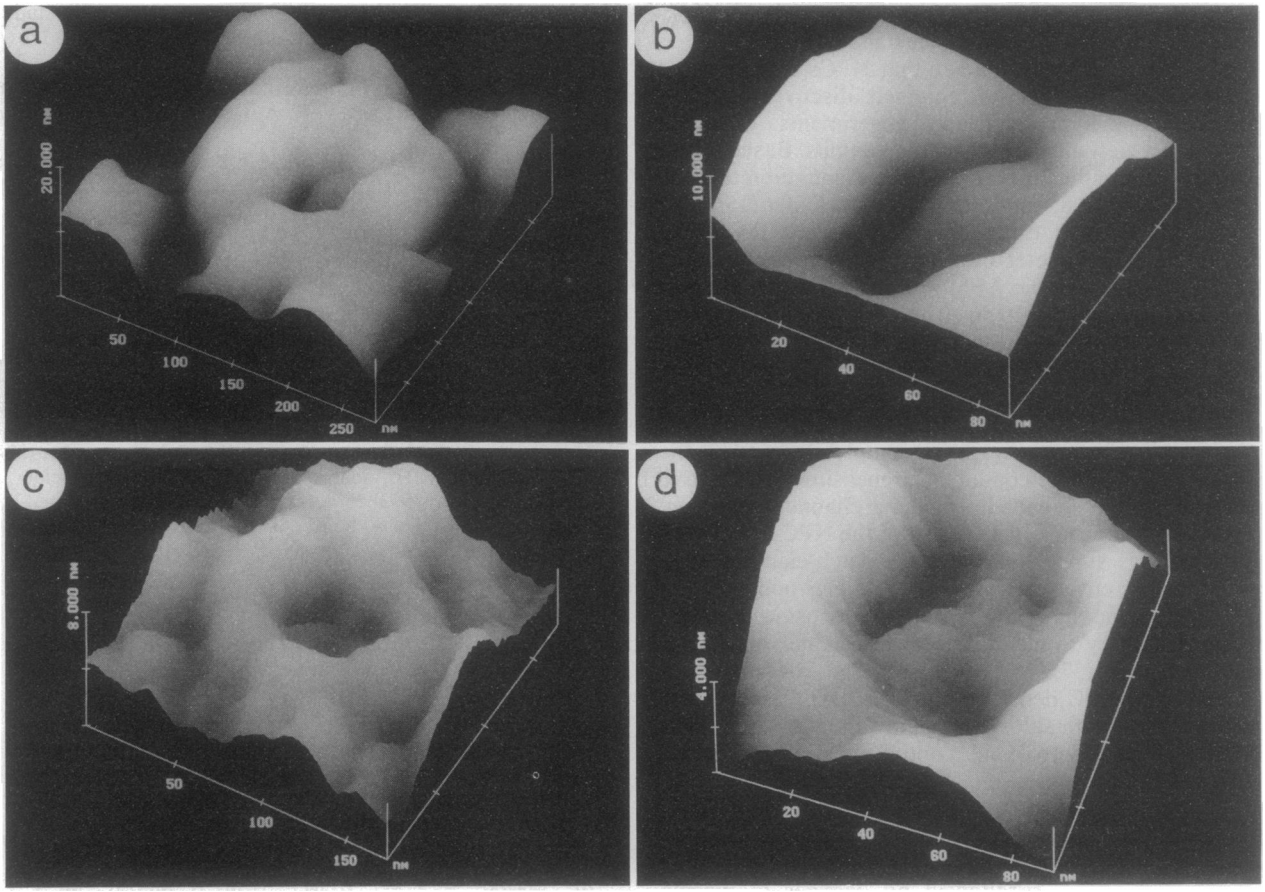

FIG. 2. Images of two individual NPCs. (*a*) Octagonal substructure of the cytoplasmically oriented outer ring can be vaguely identified. (*b*) View into the central channel of the NPC displayed in *a*. The outer diameter of the central channel is about 30 nm. Solid material, probably the putative transporter, is plugging the channel. (*c*) Another NPC with an even wider central channel entrance. Segmentation of the outer ring is detectable. (*d*) Channel entrance of NPC displayed in *c*. The 40-nm channel entrance appears plugged a few nanometers below the outer rim of the NPC.

dicates that NPCs play a key role in nucleocytoplasmic transport. However, data on specific NPC transport mechanisms are yet unclear. Nuclear electrophysiology provided specific data on the potential function of the NPCs (17). There, it was shown that cell nuclei from *Drosophila* salivary gland cells develop significant transenvelope electrical potential differences despite the fact that envelope conductance is several-hundred-fold higher than plasma membrane conductance. Based on the uptake of dextrans of variable molecular sizes, the functional diameter of the NPCs was calculated to be 9 nm. It was postulated that particles too large to diffuse through the 9-nm pore have to undergo conformational changes, or the NPC itself has to change its permeability (18). Some years later, it became apparent that nuclear protein import depends strictly on the presence of a nuclear localization signal consisting of a specific sequence of seven basic amino acids (19). More recently, patch clamp techniques were applied to the nuclear envelope, and a variety of ion channels was detected (20–23). Since the outer membrane of the nuclear envelope is in direct connection with the endoplasmic reticulum, which is a membranous compartment with known ion-channel activity (24), the presence of nuclear ion channels was not unexpected. There is accumulating evidence that ion channels could serve as constitutive components in the complicated structure of the NPCs (reviewed in ref. 25). This exciting view is supported also by the supramolecular architecture of NPCs (4, 15, 26).

We tried a different approach to directly correlate structure with function. We combined the quantitative and qualitative results of our AFM study with electrical measurements in the same preparation (Table 1). We collected data of nuclei of aldosterone-depleted and -supplemented cells. First, we analyzed pore frequency under both conditions. We randomly scanned portions of the apical nuclear surface and extrapolated the measurements of numerous small areas to total nuclear surface (see *Methods*). Since the basolateral portion of the nuclear surface was inaccessible for scanning, we assumed that pore frequency was similar all over the nuclear envelope. Six hours of exposure to aldosterone significantly increased the number of pores per nucleus, although nuclear surface remained unchanged. To our view this shows that a steroid hormone can interfere with NPC turnover. Plasma ion channels, ion carriers, and ATP-driven transporters are known to be activated by aldosterone in a delicate time sequence, either by inserting new transport proteins in the plasma membrane or by activating quiescent transporters already present (but functionally dormant) in the membrane. This was shown for Na^+/H^+ exchange (27–29), for K^+ channels (30, 31), for Na^+ channels (32), for the H^+-ATPase (33, 34), for the H^+/K^+-ATPase (35), and for the Na^+/K^+-ATPase (36). The present results indicate that aldosterone increased NPC density, while the biophysical properties of individual NPCs remained unchanged. This view is strongly supported by the virtually identical single-NPC conductance that was calculated for hormone-depleted and hormone-substituted cells. We found a conductance value close to 1 nS per individual NPC. This represents a mean value calculated from the number of pores per nucleus and from overall nuclear envelope conductance. This individual pore conductance could be an overestimation because our calculations

were based on the assumption that NPCs were the only conductive pathway between nucleus and cytoplasm.

There is accumulating evidence that NPCs represent the substrate for the nuclear ion channels discovered in the nuclear envelope by patch–clamp experiments. Our data confirm such a view and add some more details. Based on the measured NPC conductance and on the assumption that the central channel is an 80-nm-long aqueous cylinder (15) filled with isotonic solution (fluid resistivity = 100 Ω·cm), an electrical channel diameter of close to 11 nm is calculated (Table 1). However, in the AFM images, we detect channel entrance diameters of 30–40 nm. Therefore, we must assume that a major portion of the central channel is electrically blocked along its vertical axis. Current data visualizing a putative nuclear pore transporter (16) and our present AFM images support this view. Theoretically, in our experiments the nuclear transporter could have completely blocked the central channel, and the conductance measured could have originated from the so-called peripheral channels that have been described to be an intrinsic part of the NPC framework (4). This view is supported by recent patch-clamp experiments in nuclear envelopes of *Xenopus laevis* oocytes indicating that organic substrates such as adenosine trisphosphate are necessary to maintain central channels in a functionally open state (37).

We measured NPC density per nucleus only after a 6-hr incubation period with aldosterone and compared the results with the respective control values obtained from aldosterone-depleted cells. If the increase in NPC density were a prerequisite for adequate transport of aldosterone-induced ribonucleoproteins from the nucleus into the cytosol, we would expect up-regulation of NPC density by aldosterone to come *first* (i.e., within 6 hr), followed by changes in plasma membrane properties caused by the insertion of *de novo* synthesized aldosterone-dependent transporters. Recruitment from silent cytosolic pools of plasma membrane transporters and of NPC-related proteins is expected to occur well within the 6-hr period, while aldosterone-triggered *de novo* synthesis of transporters (involving transcription, translation, and membrane insertion) is known to operate on a longer time scale (38).

Aldosterone led to a large increase of the transenvelope electrical potential difference (Table 1). This could be explained by the insertion of additional NPCs with cation-selective channel properties (20), if one assumes that inorganic cation concentration in nucleoplasm is above that found in cytosol. It is interesting to note that the density of plasma cation channels in MDCK cells is by far highest in the close vicinity of the nuclear envelope—namely, in the supranuclear portion of the apical plasma membrane (39). Thus, it is tempting to speculate whether transport proteins of the plasma membrane could also represent substructures of the NPCs. This view is supported by the fact that receptors for the lectin wheat germ agglutinin (WGA) can be identified at the cytoplasmic face of NPCs (40) as well as in the apical plasma membrane adjacent to the nucleus (39). There, the WGA receptor is supposed to be closely associated with the Na^+ channels of the plasma membrane.

Another explanation for the increase of the transenvelope electrical potential difference could be the aldosterone-induced intranuclear accumulation of negatively charged material such as freshly transcribed mRNA or local decondensation of chromatin, exposing its negatively charged DNA segments (11). Further experimentation could clarify this issue.

We are grateful to Mrs. Barbara Schuricht and Mrs. Birgit Gassner for excellent technical assistance. We thank Mr. Peer Burshille (L.O.T.-Oriel) for supplying the NanoScope III. This study was supported by the Deutsche Forschungsgemeinschaft [SFB 176 (A 6)].

1. Zasloff, M. (1983) *Proc. Natl. Acad. Sci. USA* **80**, 6436–6440.
2. Dingwall, C. & Laskey, R. A. (1986) *Annu. Rev. Cell Biol.* **2**, 367–391.
3. Hanover, J. A. (1992) *FASEB J.* **6**, 2288–2295.
4. Hinshaw, J. E., Carragher, B. O. & Milligan, R. A. (1992) *Cell* **69**, 1133–1141.
5. Akey, Ch. W. (1989) *J. Cell Biol.* **109**, 955–970.
6. Hoh, J. H. & Hansma, P. K. (1992) *Trends Cell Biol.* **2**, 208–213.
7. Radmacher, M., Tillmann, R. W., Fritz, M. & Gaub, H. E. (1992) *Science* **257**, 1900–1905.
8. Oberleithner, H., Giebisch, G. & Geibel, J. (1993) *Pflügers Arch.* **425**, 506–510.
9. Gekle, M., Wünsch, S., Oberleithner, H. & Silbernagl, S. (1994) *Pflügers Arch.*, in press.
10. Birnie, G. D. & Graham, S. V. (1986) *Cell Nucleus* **11**, 182–201.
11. Oberleithner, H., Schuricht, B., Wünsch, S., Schneider, S. & Püschel, B. (1993) *Pflügers Arch.* **423**, 88–96.
12. Butt, H.-J., Wolff, E. K., Gould, S. A. C., Northern, B. D., Peterson, C. M. & Hansma, P. K. (1990) *J. Struct. Biol.* **105**, 54–61.
13. Rossier, B. C., Paccolat, M. P., Verrey, F., Kraehenbühl, J.-P. & Geering, K. (1985) *Horm. Cell Regul.* **9**, 209–225.
14. Oberleithner, H. (1991) *Cell. Physiol. Biochem.* **1**, 2–12.
15. Akey, Ch. W. & Radermacher, M. (1993) *J. Cell Biol.* **122**, 1–19.
16. Akey, Ch. W. (1990) *Biophys. J.* **58**, 341–355.
17. Loewenstein, W. R. & Kanno, Y. (1963) *J. Cell Biol.* **16**, 421–425.
18. Paine, P. L., Moore, L. C. & Horowitz, S. B. (1975) *Nature (London)* **254**, 109–114.
19. Kalderon, D., Richardson, W. D., Markham, A. F. & Smith, A. E. (1984) *Nature (London)* **311**, 33–38.
20. Matzke, A. J. M., Weiger, T. M. & Matzke, M. A. (1990) *FEBS Lett.* **271**, 161–164.
21. Mazzanti, M., DeFelice, L. J., Cohen, J. & Malter, H. (1990) *Nature (London)* **343**, 764–767.
22. Bustamante, J. O. (1993) *Biophys. J.* **64**, 1735–1749.
23. Innocenti, B. & Mazzanti, M. (1993) *J. Membr. Biol.* **131**, 137–142.
24. Schmid, A., Gögelein, H., Kemmer, T. P. & Schulz, I. (1988) *J. Membr. Biol.* **104**, 275–282.
25. Bustamante, J. O. (1994) *J. Membr. Biol.* **138**, 105–112.
26. Pante, N. & Aebi, U. (1993) *J. Cell Biol.* **122**, 977–984.
27. Oberleithner, H., Weigt, M., Westphale, H.-J. & Wang, W. (1987) *Proc. Natl. Acad. Sci. USA* **84**, 1464–1468.
28. Vilella, S., Guerra, L., Helmle-Kolb, C. & Murer, H. (1992) *Pflügers Arch.* **422**, 9–15.
29. Wehling, M., Käsmayr, J. & Theisen, K. (1991) *Am. J. Physiol.* **260**, 719–726.
30. Wang, W., Henderson, R. M., Geibel, J., White, S. & Giebisch, G. (1989) *J. Membr. Biol.* **111**, 277–289.
31. Horisberger, J.-D. (1992) *Am. J. Physiol.* **263**, 384–388.
32. Pacha, J., Frindt, G., Antonian, L., Silver, R. B. & Palmer, L. G. (1993) *J. Gen. Physiol.* **102**, 25–42.
33. Al-Awqati, Q., Norby, L. H., Mueller, A. & Steinmetz, P. R. (1976) *J. Clin. Invest.* **58**, 351–358.
34. Harvey, B. J. (1992) *J. Exp. Biol.* **172**, 289–309.
35. Oberleithner, H., Steigner, W., Silbernagl, S., Vogel, U., Gstraunthaler, G. & Pfaller, W. (1990) *Pflügers Arch.* **416**, 540–547.
36. Verrey, F., Schaerer, E., Zoerkler, P., Paccolat, M. P., Geering, K., Kraehenbühl, J. P. & Rossier, B. C. (1987) *J. Cell Biol.* **104**, 1231–1237.
37. Mazzanti, M., Innocenti, B. & Rigatelli, M. (1994) *FASEB J.* **8**, 231–236.
38. Schwab, A. & Oberleithner, H. (1994) in *Genomic and Non-genomic Effects of Aldosterone: Modern Concepts of Steroid Action*, ed. Wehling, M. (CRC, Boca Raton, FL), in press.
39. Oberleithner, H., Wünsch, S. & Schneider, S. (1992) *Proc. Natl. Acad. Sci. USA* **89**, 241–245.
40. Finlay, D. R., Newmeyer, D., Price, T. M. & Forbes, D. J. (1987) *J. Cell Biol.* **104**, 189–200.